Assessment of the oil scoop capture efficiency in high speed rotors

Paloma Paleo Cageao
Paloma.Paleo@nottingham.ac.uk
Gas Turbine and Transmissions Research Centre
University of Nottingham, UK

Kathy Simmons *
kathy.simmons@nottingham.ac.uk
Gas Turbine and Transmissions Research Centre
University of Nottingham, UK

Arun Prabhakar
arun.prabhakar@nottingham.ac.uk
Gas Turbine and Transmissions Research Centre
University of Nottingham, UK

Budi Chandra
budi.chandra@uwe.ac.uk
University of West England, UK

Experimental research was conducted into a scooped rotor system that captures oil from a stationary jet and directs it through passages within the shaft to another axial location. Such a system has benefits for delivering oil via under-race feed to aeroengine bearings where direct access is limited. Oil capture efficiency was calculated for three jet configurations, a range of geometric variations relative to a baseline and a range of operating conditions. Flow visualization techniques yielded high-speed imaging in the vicinity of the scoop leading edge.

Overall capture efficiency depends on the amount of oil initially captured by the scoop that is retained. Observation shows that when the jet hits the tip of a scoop element, it is sliced and deflected upwards in a 'plume'. Ligaments and drops formed from this plume are not captured. In addition, some oil initially captured is flung outwards as a consequence of centrifugal force. Although in principle capture of the entire supply is possible over most of the shaft speed range, as demonstrated by a simplified geometric model, in practice 60% to 70% is typical.

Significant improvement in capture efficiency was obtained with a lower jet angle (more radial) compared to baseline. Higher capture efficiencies were found where the ratio of jet to scoop tip speed was lower.

This research confirms the capability of a scoop system to capture and retain delivered oil. Additional numerical and experimental work, is recommended to further optimise the geometry and increase the investigated temperature and pressure ranges.

NOMENCLATURE

α	Jet deflection angle (deg)
η	Capture efficiency (%)
θ_2	Angle (defined in Fig. 4) (deg)
θ_4	Angle (defined in Fig. 4 (deg)
θ_{jet}	Jet orientation angle (deg)
θ_{loss}	Angle related to uncaptured jet oil jet (defined in Fig. 4) (deg)
θ_{ref}	Baseline jet orientation angle (deg)
ν	Oil kinematic viscosity ($m^2 s^{-1}$)
ρ	Oil density at 30 °C ($kg m^{-3}$)
ρ_j	Oil density at observation j ($kg m^{-3}$)
σ	Oil/air surface tension ($N m^{-1}$)
ω	Rotational shaft speed (rpm)
ω_{max}	Maximum shaft speed tested (rpm)

*Address all correspondence to this author.

A,B,C	Positions defined in Fig. 4
d_c^{ref}	Baseline size of oil scoop constriction (m)
d_c	Size of oil scoop constriction (m)
d_c*	Non-dimensional size of oil scoop constriction
fps	Frames per second
n_j	Sample size
n_{scoops}	Number of scoop blades
Q_{jet}	Oil jet flow rate ($\mathrm{l\,min^{-1}}$)
$\overline{\dot{M}}_{jet}$	Average of oil jet mass flow rate ($\mathrm{kg\,s^{-1}}$)
$\dot{M}_{scoop}$	Oil mass flow rate through scoop ($\mathrm{kg\,s^{-1}}$)
$\dot{M}_{jet}$	Oil jet mass flow rate ($\mathrm{kg\,s^{-1}}$)
R_{tip}	Rotor outer radius (m)
R_{jet}	Radial distance to oil injector (m)
$R_c{}^2$	Coeffcient of determination
ROI	Region of interest
T_{jet}	Feed oil temperature (°C)
V_j	Oil jet velocity ($\mathrm{m\,s^{-1}}$)
VR	Jet to scoop tip velocity ratio
VR_{thr}	Threshold velocity ratio

1 Introduction

Lubrication and cooling of transmission systems components in a gas turbine engine is a prime concern. This is particularly important for the bearings where appropriate oil supply will ensure safe, reliable and efficient engine operation and a long life expectancy. The oil lubrication system is designed to minimize the effects of friction and wear and to provide cooling both to the bearings and to the surrounding bearing chambers. In civil aero-engines, which have shafts rotating at high speeds up to 15.000 rpm, it is common practice to use jet lubrication for bearings. Oil is targeted at the annulus gap between the inner and outer race [1] or at collection scallops for under-race feed. These are illustrated conceptually in Fig. 1. As speeds rise, centrifugal forces increase and it becomes more difficult for oil targeted directly at the bearing to penetrate to the critical surfaces. Consequently, in high duty conditions (high speeds, loads and operating temperatures) to ensure the oil flow to the bearings is effective and efficient, under-race lubrication is often preferred [1, 2, 3]. With under-race feed, oil moves outwards through feed holes within the shaft to lubricate the inner race surfaces of the bearing under the influence of centrifugal force. Under-race lubrication presents several advantages for higher speed applications, but in a confined space there may not be sufficient axial access for the jet to target the under-race location directly and in such case it is desirable to supply the oil at a different axial location to that of the feed, transporting the oil to the bearing through slots in the rotor. In such cases, one configuration proposed is a rotating 'scoop geometry' device, where each scoop captures a charge of lubricant as the shaft rotates delivering it to a bearing as an under-race feed. Such a geometry is illustrated conceptually in Fig. 2 and 3.

The concept of a scoop delivery system is not new; Brown [3] in 1970 described a scoop system where an oil jet is targeted axially at a channel that delivers oil to under-race

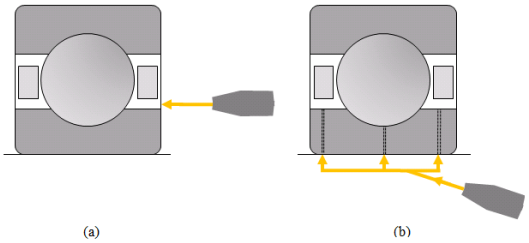

Fig. 1: Oil jet targeted directly at bearing a) shows oil targeted directly at a bearing but b) shows under-race feed.

feed holes at a different axial location, but development has been relatively slow as in most cases a scoop delivery system is not necessary. An early scoop design for a gas turbine is described in the 1987 patent of Kovaleski [4]. The invention described is a scoop system that directs specific proportions of oil axially, forward and rearward from the scoop to lubricate bearings located on opposite sides of the scoop itself. Over the years, scoop geometry design has evolved. The patents of Fisher et al. [5] and Fisher [6] are for conventional flat bladed scoops whereas that of Dins et al [7] describes a scoop comprising a curved blade intended to maximize fluid capture. In 2016 Rolls-Royce patented the concept of a bi-directional scoop [8] where the key difference to previously patented scoop designs is that the oil inlet path through the scoop follows a path angled such that it is turning throughout its journey rather than travelling first perpendicular to the shaft and then parallel to it.

Continuously increasing demands on gas turbine engines for increased fuel efficiency and lower environmental impact are leading to more compact and lighter engines [9]. Without a doubt, the desire for increased compactness leads to more crowded components making an appropriate, effective and efficient lubrication system even more challenging. Where bearing lubrication is concerned it is therefore important that as much as possible of the oil delivered by the jet subsequently arrives at the bearing. The ratio of the oil captured by the scoop to the amount directed at the scoop from the stationary nozzle is commonly termed the oil scoop capture efficiency. In the ideal scenario all the oil exiting the nozzle would travel to the target component. Capture efficiency can depend on a wide range of parameters such as the shaft speed, oil jet characteristics (including configuration, orientation, velocity, distance travelled by the oil jet and flow rate) and the geometry of the scoop device (including number, angle and profile of the blades/scoops and the geometry of the oil passages along the shaft). Oil scoops with higher efficiency could permit a decrease in the total amount of oil that must be delivered to the jet which may in turn allow reduction in the size and weight of parts of the oil system.

In this paper the results from an experimental investigation into a scoop geometry are presented. Geometric variations of the nozzle and scoop geometries are investigated over a range of operating conditions using a test module mounted to a single shaft test facility at the University of Nottingham's Gas Turbine and Transmissions Research Centre (G2TRC). The value of such data is two-fold with numer-

ical and visualisation data providing direct design insight and also supporting modelling capability through qualitative and quantitative validation.

2 Previous Work

There are a couple of published Computational Fluid Dynamics (CFD) investigations into aero-engine scoops. The first of these is by Prasad et al. [10] where a system involving two scoops and two nozzles was investigated. The paper gives very little geometric data but the scoop is sharp edged and does not look too dissimilar to those investigated here. For fixed shaft speed the effect of increasing the oil flow rate (through increasing the jet velocity) was to increase capture efficiency but the effect was quite small with only 5% increase in capture efficiency for a fivefold increase in jet velocity. For fixed jet velocity and increasing shaft speed up to 4 times baseline, the capture efficiency increased to a peak value, 8% above baseline when the shaft speed was double the baseline shaft speed. The authors also found that increasing the scoop system width by 50% increased capture efficiency by 12%. Another result presented is that a 60% increase in capture efficiency could be obtained by reducing the scoop outer diameter by 10%, this being attributed to reduced magnitude of centrifugal force. Although no experimental data is included in the paper the authors state that their CFD data matches experiment to within 2%.

Korsukova et al. [11] conducted a numerical investigation on a geometry very similar to that investigated experimentally here using both CFD and smooth particle hydrodynamics (SPH). The 2-D, 2-D extrusion and 3-D models provide significant insight into flow behaviour near the scoops. The paper highlights a couple of key features, that were also seen experimentally. First, the formation of plume, droplets and ligaments after the oil jet is sliced by the scoop that are not captured by the scoop system. Second, part of the oil initially captured is subsequently expelled as a consequence of centrifugal forces. Both represent losses and reduce the capture efficiency. In the paper the simulation data is compared with included experimental data showing good qualitative agreement and a quantitative agreement to within 10%.

There does not appear to be any published experimental work relating to scoop systems similar to the one investigated here. In particular the experimental work mentioned in [10] is not currently in the public domain.

3 Oil scoop geometry investigated

In the scoop geometry investigated here a rotating radial scoop similar in geometry to that proposed in US patent 6,682,222 [6] is used to capture oil from a stationary oil jet. In the patented scoop, oil is directed towards the scoops on a trajectory dictated by the nozzle orientation, with the nozzle axis mounted at an angle θ_{jet} to the extended radius as illustrated in Fig. 2. The intention for the patented device is that some oil is captured by the scoops and some is reflected back into the chamber for a second lubrication purpose. In the current investigation the intention is to capture as much oil as possible in the scoops.

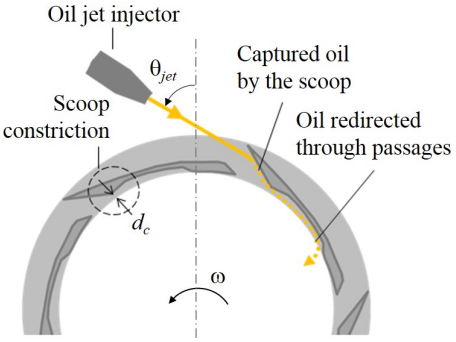

Fig. 2: Side view of scoop system (illustrative geometry).

This leads to the concept of capture efficiency as the ratio of oil captured by the scoops to oil delivered by the jet. There are two elements to be considered with regard to oil capture. The first is how much of the oil from the jet could potentially be captured; this is essentially the amount of oil that falls within the zone swept by the scoops. Dependent on many geometric and operational parameters this value can be 100% of the delivered oil. The second element is how much of this initially captured oil is ultimately delivered along the axial passages. Not all the oil initially captured is retained by the scoop system; some will flow back out of the scoops as centrifugal forces overcome initial fluid momentum.

Once captured the oil is directed axially and in a potential application of the device it would subsequently be delivered to an engine component such as a bearing via under-race feed as conceptually illustrated in Fig. 3. In the experimental investigation conducted here, captured oil was delivered to a measurement system, not to a bearing.

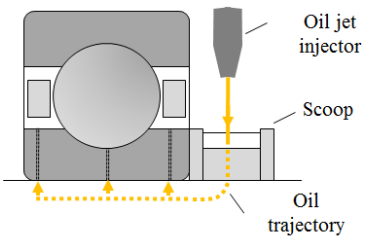

Fig. 3: Front view of scoop system (illustrative geometry).

As shown in Fig. 2, the oil injector ejects a jet of oil across open space toward the scoop and against rotation ω taking advantage of the oil's inertia to drive the oil inwards towards the axial passages. Because the scoops are rotating, centrifugal forces act to drive the oil outwards and an identified element of the scoop system is the constriction labelled on Fig. 2. As identified in [6] this constriction is not just a barrier to oil flowing backwards out of the oil passages, it

also creates an adverse centrifugal pressure gradient to further deter escape of captured oil. The effect on scoop capture efficiency of the radial size of the narrowest part of the constriction, d_c, is one of the parameters investigated in this study. The jet angle, θ_{jet}, is another experimentally investigated parameter.

In this study a geometry comprising 6 scoops was chosen. Over the parametric range of shaft speeds and oil flowrates three jet angles were investigated and these are the baseline θ_{ref} (64.2°), $\theta_{ref} - 5°$ and $\theta_{ref} - 10°$.

3.1 Simplifed model

In seeking to better understand how the scoop system works and what are the key parameters, a simplified model has been developed. The simplified scoop system geometry is illustrated in Fig. 4, where the scoop blades are represented by a simple wedge shape. In this geometrical analysis the jet is represented as a line, having neither width nor spread angle. The formation of plumes, drops and ligaments is not considered and all the oil initially captured by the scoop is assumed retained. The jet is sliced when the scoop tip is at point A, while the next scoop is at point C (light grey wedges). As the scoop system rotates (dark grey wedges) the jet grows from point A to point B.

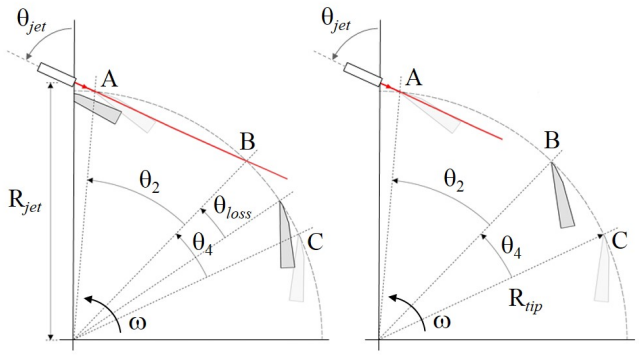

Fig. 4: Capture criterion. (a) At $VR < VR_{thr}$, the oil jet passes point B before next scoop reaches there. The oil jet is not entirely captured. (b) At $VR \geq VR_{thr}$, the scoop passes point B before the oil jet. The oil jet is entirely captured.

It is useful here to introduce the velocity ratio VR, a dimensionless parameter defined as the ratio of the scoop tip velocity to the jet velocity:

$$VR = \frac{\omega R_{tip}}{V_j}, \tag{1}$$

where R_{tip} is the rotor outer radius, V_j the oil jet velocity and R_{jet} is the distance of the oil injector from the centre of the rotor.

At low velocity ratios the jet cuts the circle formed by the outer radius of the scoop at point B before the next scoop has reached there (Fig. 4a). The section of the jet outside of the sweep of the scoop is not captured; this oil loss is represented by θ_{loss} in Fig. 4a. At a threshold capture velocity ratio VR_{thr}, the tip of the next scoop meets point B at the same instant as the jet. This threshold velocity ratio is given by

$$VR_{thr} = \frac{\theta_4 V_j}{\omega_{thr} 2 R_{tip} \sin\left(\frac{\theta_2}{2}\right)}. \tag{2}$$

Above VR_{thr}, the jet is theoretically fully captured and for the investigated geometry $VR_{thr} = 0.44$, calculated using Eq. (2).

As long as the scoops are rotating (shaft speed $\omega > 0$) the oil capture efficiency in the region $VR < VR_{thr}$ is given by:

$$\eta = \frac{\frac{2\pi}{n_{scoops}} - \theta_{loss}}{\frac{2\pi}{n_{scoops}}}, \tag{3}$$

where n_{scoops} is the number of scoop blades and $2\pi/n_{scoops} = \theta_2 + \theta_4$ is the angle between scoops (see Fig. 4). θ_{loss} is defined as

$$\theta_{loss} = \theta_4 - 2\,VR_{thr} \sin\left(\frac{\theta_2}{2}\right), \tag{4}$$

and the angle θ_2 is

$$\cos\left(\frac{\theta_2}{2}\right) = \frac{R_{jet}}{R_{tip}} \sin\left(\theta_{jet}\right). \tag{5}$$

Thus it can be seen that in the low speed region the capture efficiency depends on the number of scoops, jet angle and velocity ratio.

This simplified geometrical model was developed to give insight into the oil capture process. The model does not include any losses due to pluming, droplet and ligament formation or centrifugal forces and because it is a 2D model it is equally valid for any of the jet configuration tested in this work: single jet, twin jets and tandem jet (jet configurations are discussed in Section 4.3). The twin jet configuration is two single jets side by side and the tandem jets are two single jets with an angular offset. If jet interaction effects are neglected then the model can be applied additively for these two-jet configurations.

4 Experimental test rig

The laboratory experiments were conducted using a scoop test module mounted onto the G2TRC single shaft test facility. The facility consists of a bed plate, gearbox and 130 kW DC motor that can rotate the bearing-mounted shaft up to 15.000 rpm dependent on the installed test module. In these tests the maximum shaft speed (ω_{max}) was limited to 10.000 rpm. A schematic diagram of the facility with test module mounted is shown in Fig. 5. In these tests shaft speed was set as a direct setpoint input to the motor drive, with an estimated uncertainty of ± 4 rpm at all setpoints based on measured data analysis.

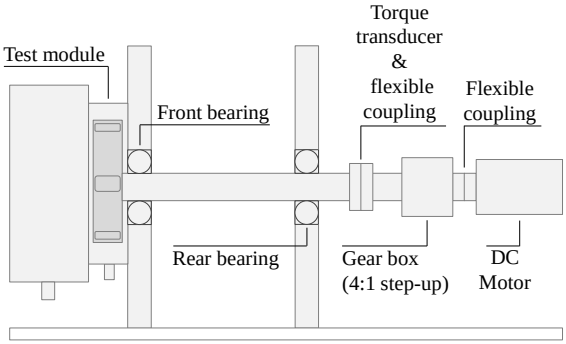

Fig. 5: Schematic illustration of the single shaft test facility with scoop module mounted.

The scoop test module consisted of two chambers, the scoop chamber containing the jet and scoop geometry and the front chamber. Oil caught by the individual scoops was directed axially along the shaft through passages and collected in the front chamber. Each chamber has its own scavenge port so that oil passing through the scoops is separated from oil not captured by the system. A schematic illustration of the oil scoop test module and associated hydraulic circuit is shown in Fig. 6. The first build of the test module had a front chamber that was too small in diameter leading to scavenge issues and a larger Perspex^{TM} chamber was added outside the original stainless steel front chamber. Both can be seen in the photographs of the test module shown in Fig. 7.

A positive displacement pump delivers oil to the oil jet manifold at the required flow rate Q_{jet}. The flow rate was changed manually as required for each test as an input value to the pump inverter and measured using an Kral flowmeter (OME24) that has a range up to 50 l min^{-1}. For these experiments MIL-PRF 7808 turbine oil type was used, with the steady state feed temperature T_{jet} controlled to be close to 30 °C. The kinematic viscosity and density of the oil at 30 °C are 2.71×10^{-5} m^2 s^{-1} and 933.4 kg m^{-3} respectively and oil/air surface tension is 3.12×10^{-2} N m^{-1}.

The front chamber contains an exit port at the bottom through which oil exits under the effect of gravity via a flexible pipe into a container standing on electronic scales. The mass of oil on the scales is logged during testing and that data is used to calculate the captured oil flowrate. The oil

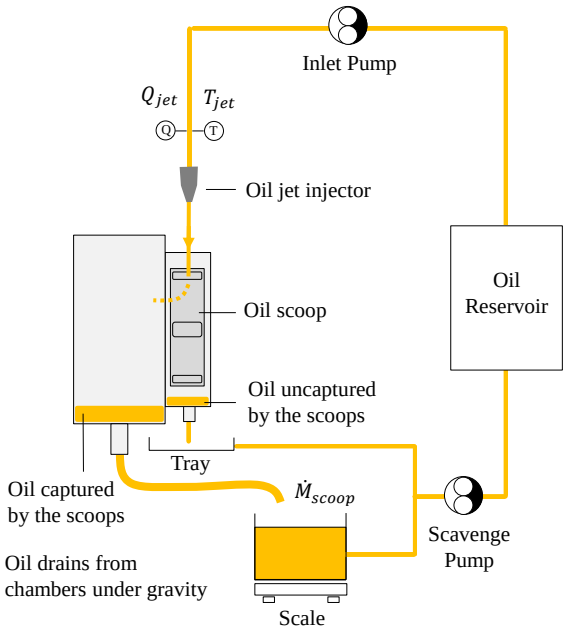

Fig. 6: Schematic illustration of the oil scoop module and associated hydraulic circuit.

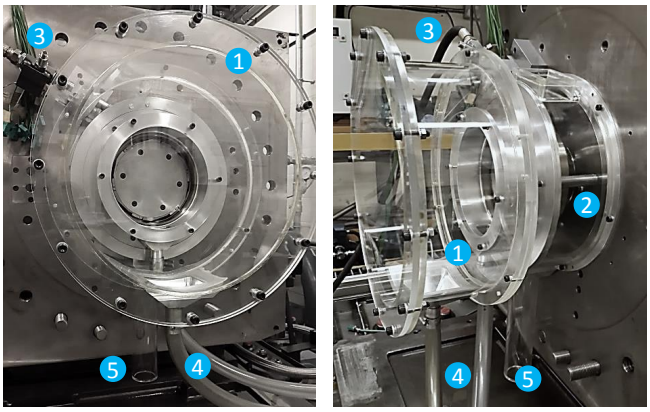

Fig. 7: Oil scoop test module: side view (left) and front view (right). 1-Front chamber, 2-Scoop chamber, 3- Oil jet injector, 4-Front chamber exit and 5-Scoop chamber drain.

flow rate out of the front chambers was measured at each test point. A positive displacement pump was used to empty the container after each test returning the oil to the oil reservoir.

The scoop chamber houses the rotating scoop element and the housing contains an exit port that provides gravity drainage for the oil not passing through the scoops. Lubrication oil for the rig front bearing also exits here. Oil leaving through the scoop chamber housing is collected in a tray and pumped back to the oil reservoir. The top of the circular cross-section scoop chamber contains an opening with a cover for an access to the interior of the chamber allowing easy access with the borescope for flow visualization.

4.1 Oil scoop capture efficiency calculation method

At first start-up the rig was allowed to warm-up and was then observed to operate in a steady, stable condition at each setpoint. At each test point, after changing the operating conditions, 1-2 minutes of settling time were allowed to reach a stable operating condition. Rig monitors were used to assess when conditions had stabilised. Once the rig was stabilised at the setpoint oil was collected in the collection tank for a period of 5-8 minutes. Throughout the test, oil flowrate and temperature were logged along with the mass of oil on the scales.

The oil scoop capture efficiency is the ratio of the oil mass flow captured (and retained) by the scoop $\dot{M}_{scoop}$ to the average of the overall mass flow of oil that was injected to the scoop during the test $\overline{\dot{M}}_{jet}$, that is

$$\text{Efficiency}[\%] = \frac{\dot{M}_{scoop}[\text{kg s}^{-1}]}{\overline{\dot{M}}_{jet}[\text{kg s}^{-1}]}, \tag{6}$$

The mass of the collected oil through the scoops (m) was measured and recorded at a sampling rate of 4 Hz. A simple linear regression analysis using the least squares method was calculated to determine the oil mass flow rate $\dot{M}_{scoop}$, represented by the slope or regression coefficient of the fitted line. The coefficient of determination ${R_c}^2$ obtained in the tests varied between 0.999 and 1 indicating that the line fit was straight with an excellent fit and therefore the mass flow rate was steady throughout the test.

The electronic scales were calibrated to $\pm 5g$ and at the lowest flowrate the minimum mass collected over the duration of a test was 4kg. Combining uncertainties we find the maximum uncertainty in $\dot{M}_{scoop}$ to be 0.1%.

The average mass flow rate of oil injected to the scoops is expressed by

$$\overline{\dot{M}}_{jet} = \sum_{j=1}^{n_2} \dot{M}_{jet_j} = \sum_{j=1}^{n_2} \rho_j Q_{jet_j}, \tag{7}$$

where $\rho_j = f(T_{jet_j})$ is the density of the oil at observation j; a function of the oil feed temperature T_{jet_j}. Q_{jet_j} is the oil jet manifold flow rate at observation j of n_j measurements at a sampling rate of 1 Hz to ensure the system was steady stable through each test.

Calibration data for the flowmeter gives a maximum uncertainty in volume flowrate of 0.6%. The uncertainty in density is the product both of the variation in supply temperature and also the accuracy of the correlation used to give density as a function of temperature. Oil supply temperature was measured using K-type thermocouples with a quoted accuracy of $\pm 2K$ and our data shows the supply temperature to have varied by less than 0.6K over the duration of the tests. Using available oil property data gives us an uncertainty in density of 1.5% based primarily on thermocouple accuracy. Combining the uncertainties in volume flowrate and density yields an uncertainty of around 1.6% in $\overline{\dot{M}}_{jet}$. Combining the uncertainties in jet mass flowrate and scoop captured mass flowrate gives a representative upper limit on uncertainty in capture efficiency of around 1.6%, dominated by the uncertainty in supply oil density.

An additional consideration for an experimental study of this kind is repeatability, a measure of the extent to which identical results would be produced at the same nominal set point if a test were repeated. The time available for testing precluded the possibility of any kind of full statistical analysis. However, to give an indication, one of the tests (twin jet, constriction ratio 1 and $\theta_{ref} - 5°$) was repeated on two different days, before and after a rig rebuild. The two data sets are shown plotted in Fig. 8 where it can be seen that the points are almost indistinguishable. The average difference between values is 0.5% with the maximum difference of 1.5% occurring at $\omega/\omega_{max} = 0.1$. This value is less than the estimated measurement uncertainty. The only parameters that would vary from test to test not accounted for in the measurements made are the air properties.

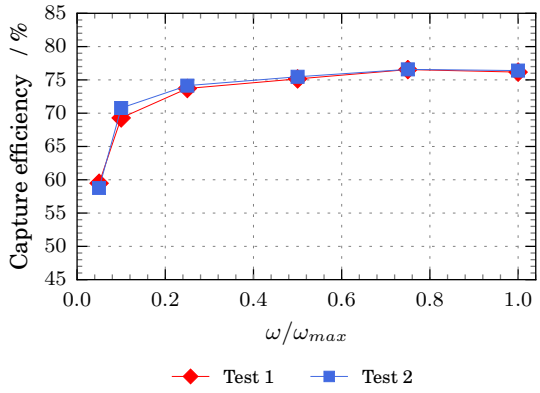

Fig. 8: Repeat test indicating level of repeatability. Test configuration: Tandem jet, d_c^*= 1 and $\theta_{jet} = \theta_{ref} - 5$.

4.2 Visualization

Visualization of the oil jet behaviour in the vicinity of the leading edge of the scoop was also conducted. Fig. 9a shows the set-up for the visualization during the experiments. For the image acquisition a high speed camera (manufactured by IDT, model OS4-S3-M-04) was used. The camera is 12 bit monochrome, with 1024x1024 pixel resolution and can acquire images at up 6000 frames per second (fps). Higher frame rates can be obtained if the image resolution is reduced. The camera has 8 GB onboard RAM and 512 GB Solid State Memory. The images were recorded using IDT's Motion Studio software. To improve the resolution and quality of images of the interior of the scoop chamber an Olympus series 5 zoom swing prism rigid borescope was attached to the camera. The borescope has an 8 mm diameter and 54 cm working length; the direction of view is 45° to 115°

downwards from the borescope axis and the field of view is 50° as shown in Fig. 9b. For illumination four white lights, Model 120E Veritas, were used. They were synchronized and pulsed with the high speed camera. Each light offered 22 000 lumens output when pulsed.

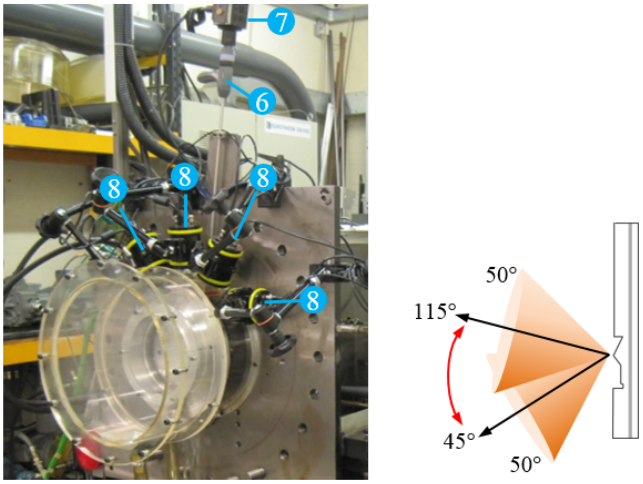

(a) (b)

Fig. 9: (a) Visualization set up. 6-Borescope, 7-Camera and 8-Lights. (b) Direction and field of view of the borescope.

The selection of the image resolution, the image acquisition rate and the illumination must be optimised at each condition. For higher shaft speeds a higher frame rate is desirable and this requires the number of pixels per frame to be reduced. With a higher frame rate it becomes harder to get enough light in the frame. During imaging, the region of interest (ROI) was adjusted appropriately, within the capability of the boroscope field of view as shown in Fig. 10. The image acquisition rate was chosen considering the shaft speed of each test in order to be able to visualize the jet flow with a good resolution, avoiding blurred images. As an example, at low shaft speeds a typical image resolution would be 512x260 pixels and a frame rate of 10 000 fps selected and at high speeds an image size of 512x128 pixels with a frame rate of 44 000 fps was employed. Visualization of the flow for high jet flow rates and/or high shaft speeds was difficult because under those circumstances, the borescope lens was constantly covered with splashed oil.

At low shaft speeds and low oil flowrates, a good understanding of flow features affecting oil scoop capture efficiency was gained by observing the oil jet interaction with the scoop leading edge. However, the visualization of the process of structural change of the jet was limited.

To observe the process of structural change of the jet including the surrounding scoop geometry a series of tests involving a simplified test module were undertaken. The simplified module consisted of a cylinder – with same inner diameter as the scoop device test module and six solid wedge elements representing the scoops. The rear end of the

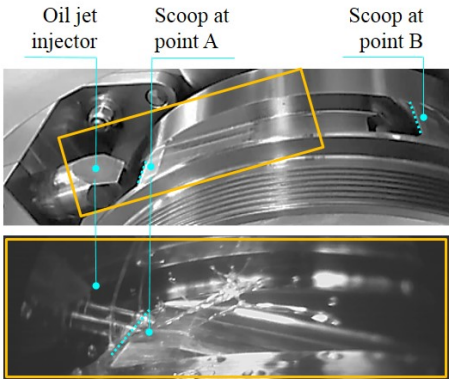

Fig. 10: Images of the scoop device and the oil jet injector. Top: The ROI is marked with a rectangle. Bottom: Frame showing the ROI from the recorded high speed filming using the borescope connected to the high speed camera.

scoop circumferential outer surface was represented by a thin wire. This geometrically simplified test module is shown in Fig. 11.

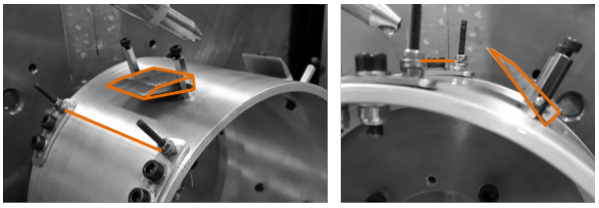

(a) (b)

Fig. 11: Geometrically simplified scoop test module. Highlighted with orange are the wedge shape and the thin wire.

4.3 Test matrix

A number of different tests were conducted on the scoop test module and these are detailed along with the relevant parametric ranges in each of the following subsections. All testing was conducted on a scoop unit consisting of 6 scoop elements similar to those illustrated in Fig. 2. A table summarising the testing conducted is included as Section 4.3.5.

4.3.1 Effect of jet to scoop velocity ratio

In the first set of tests a jet consisting of two nozzles as illustrated in Fig. 12a was used. The flowrate was set to a constant value corresponding to the highest jet velocity tested and the shaft speed ratio, defined as $\frac{\omega}{\omega_{max}}$, was varied from 0.05 to 1 in steps of 0.05. The baseline jet angle θ_{ref} was used along with a baseline scoop constriction d_c. A non-dimensional scoop constriction $d_c{}^*$ is defined as the scoop constriction ratio with reference to the baseline d_c.

4.3.2 Effect of scoop constriction

Using the same geometric configuration as in Section 4.3.1 scoop constrictions ratios $d_c{}^*$ of 1, 1.5 and 2 were investigated. As with the investigation of Section 4.3.1 the flowrate was set to a constant value (highest jet velocity tested) and shaft speed ratio was varied from 0.05 to 1 in steps of 0.05.

4.3.3 Jet velocity varying with shaft speed

In most current aero-engines the amount of oil delivered to bearing chambers and bearings is not a fixed amount but varies as a function of the speed of the shaft driving the pumps. Consequently, the velocity ratio (jet velocity to scoop tip velocity) may vary very little with shaft speed. A series of tests was conducted with an almost constant velocity ratio over a range of shaft speeds and for three scoop constriction ratio values, 0.5, 1 and 2. In these tests a different jet arrangement was used where there were two nozzles in tandem (two single orifice jets 10° apart circumferentially) as shown in Fig. 12b but the jet baseline angle was retained. To see whether the jet configuration was a significant factor the test with a constriction ratio of 1 was repeated for three jet configurations, single jet, twin jets (a nozzle with two orifices axially aligned) and tandem jets as shown in Fig. 12.

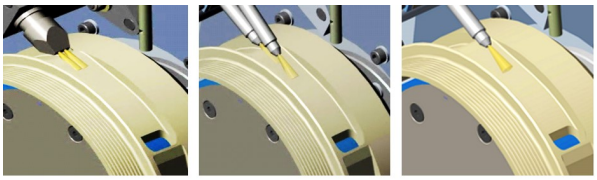

(a) (b) (c)

Fig. 12: Jet configurations tested: (a) twin jets, (b) tandem jets and (c) single jet.

4.3.4 Effect of jet angle

For the tandem jets configuration, tests were conducted with three different jet orientations: θ_{ref} as the baseline angle (see Fig. 13), $\theta_{ref} - 5°$ and $\theta_{ref} - 10°$.

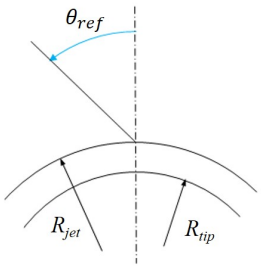

Fig. 13: Baseline oil jet orientation, θ_{ref}. Arrow defines the positive direction of the angle.

4.3.5 Summary of tests conducted

For completeness and ease of reference Section 4.3.5 is included here, summarising the conditions associated with each of the tests conducted.

5 Results and discussion

5.1 Effect of velocity ratio, fixed jet velocity

For a fixed jet velocity Fig. 14 shows how the capture efficiency varied with velocity ratio. The capture efficiency initially increases with shaft speed, reaching a maximum value at a velocity ratio between 0.8 and 1.0 with around 81% of the oil being captured by the scoops and then decreasing as shaft speed is further increased. Also on the graph is shown the theoretical maximum oil capture efficiency for an ideal scoop system. Above the total capture threshold (i.e., VR_{thr}, where $VR = 0.44$), the theoretically efficiency is 100% .

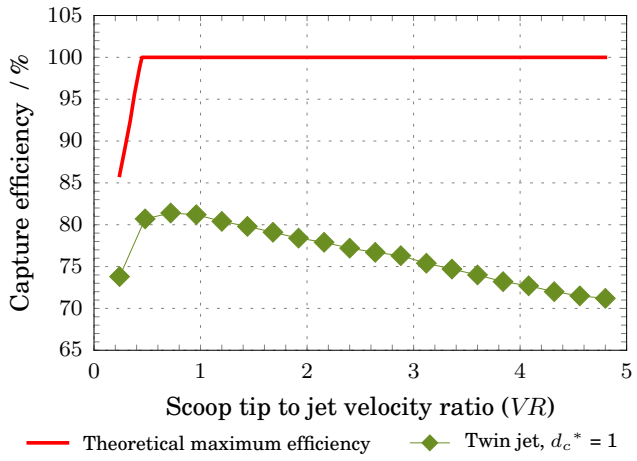

Fig. 14: Variation in capture efficiency with velocity ratio for a fixed jet velocity and varying shaft speed.

The amount of oil captured by the scoop system depends not only on how much is initially scooped but also how much is retained. Analysis of the video imaging shows that i) as the scoop approaches the jet there is an amount of oil that is deflected by the pressure field creating a flow away from the scoop and ii) as the scoop rotates a portion of oil initially scooped will be accelerated outwards through centrifugal force and will leave the scoop. These factors both increase with increasing speed thus reducing capture efficiency. Figures 15 (images from the geometrically simplified test module) and 16 (images from the representative test module) illustrate these two factors. In Fig. 15, when the jet is sliced by the wedge leading edge, the oil jet is deflected with a jet deflection angle α of approximately 135 ° from the axis line of the jet (Fig. 15b). The head of the sliced oil scrolls up gradually forming a plume (blue arrows in Fig. 15b-j). Just before the jet interacts with the next scoop, the jet deflection angle decreases to about 45 ° (Fig. 15j). The plume extends

Table 1: Parameters and conditions of the conducted tests

Test Assess effect of:	Shaft speed $\frac{\omega}{\omega_{max}}$	Velocity ratio VR	Set up configuration	Cross reference
Velocity ratio, fixed jet speed	0.05 to 1	0.3 to 5	Jet angle [θ_{jet}]: θ_{ref} Constriction [d_c^*]: 1 Jet configuration: Twin jet	Section 4.3.1 Section 5.1 Fig. 14
Scoop constriction	0.05 to 1	0.3 to 5	Jet angle [θ_{jet}]: θ_{ref} Constriction [d_c^*]: 1, 1.5, 2 Jet configuration: Twin jet	Section 4.3.2 Section 5.2 Fig. 17
Jet velocity varying with shaft speed VR almost constant	0.05 to 1	4.4 to 4.8	Jet angle [θ_{jet}]: θ_{ref} Constriction [d_c^*]: 1 Jet configuration: Twin jet	Section 4.3.3 Section 5.3 Fig. 18
Jet velocity varying with shaft speed Higher VR	0.5 to 1	4.4 to 6	Jet angle [θ_{jet}]: θ_{ref} Constriction [d_c^*]: 0.5, 1, 2 Jet configuration: Tandem jets	Section 4.3.3 Section 5.3 Fig. 19
Jet configuration	0.05 to 1	4.4 to 4.8	Jet angle [θ_{jet}]: θ_{ref} Constriction [d_c^*]: 1 Jet configuration: Twin, tandem, single	Section 4.3.3 Section 5.3 Fig. 20
Jet angle	0.5 to 1	4.4 to 6	Jet angle [θ_{jet}]: θ_{ref}, $\theta_{ref} - 5°$, $\theta_{ref} - 10°$ Constriction [d_c^*]: 1 Jet configuration: Tandem jet	Section 4.3.4 Section 5.3 Fig. 23

upwards and small ligaments and drops are formed. A significant portion of the ligaments and drops are not captured by the scoop and this represents a capture inefficiency of the scoop system. In addition, Fig. 15j shows ligaments of oil expelled from the edge of the scoop as it rotates.

In Fig. 16, when the scoop edge is approaching the jet (Fig. 16a-e), the deflected plume is observed (in Fig. 16a this is marked with a circle). Ligaments of oil leaving the edge of the scoop are well captured on the images of Fig. 16e-h. In Fig. 16e, just before the jet starts to slide along the inner scoop surface, ligaments of oil are expelled and these are marked with a ellipse. Both these factors contribute to the capture efficiency being less than 100% even though it is geometrically feasible under these conditions.

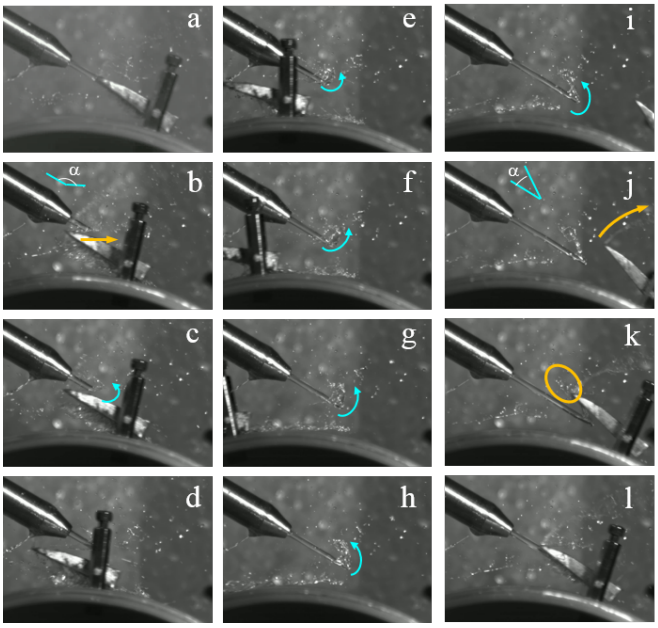

Fig. 15: Visualization of the jet flow at increments of 1×10^{-3}s with single jet for a simplified geometry of the scoop device. Angle jet is θ_{ref}, scoop construction ratio of 1 at the shaft speed ratio of 0.05 and VR of 4.3.

5.2 Effect of scoop constriction, fixed jet velocity

The results of the tests run with constant jet velocity and 3 constriction sizes are shown in Fig. 17. The graph shows that constriction size makes no difference to the shaft speed at which the maximum capture efficiency occurs but it does make a difference to the capture efficiency itself with the highest values occurring for the larger constriction value. The data for scoop constriction ratios d_c^* of 1.5 and 2 is very similar with slightly lower values for the d_c^* of 1 although in most cases the difference falls within experimental uncertainty. Overall capture efficiency is made up from the proportion of oil entering the scoops in the first place and the proportion of that, that is retained. In all three of these cases the amount of oil entering the scoop is the same and so the differences in capture efficiency can be attributed to differences in retention. As jet momentum and centrifugal forces do not vary with constriction we can conclude that the tighter constriction does limit the rate at which oil flows into the axial channels a little.

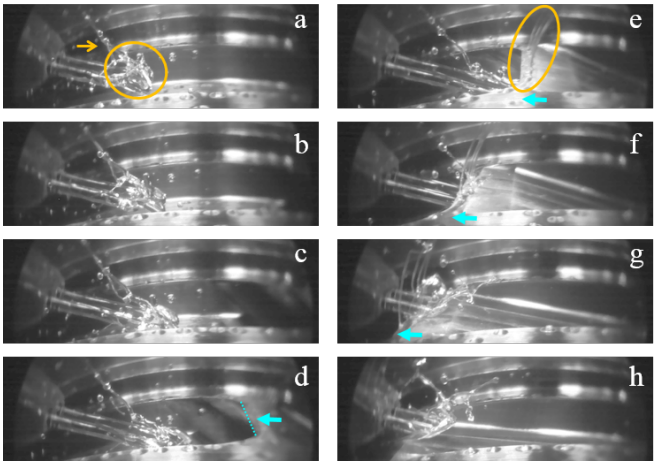

Fig. 16: Visualization of the jet flow evolution at increments of 2×10^{-3}s for a twin jet configuration. Angle jet is θ_{ref}, scoop constriction ratio of 1 at shaft speed ratio of 0.05 and VR of 4.3. The blue arrow points to the leading edge of the scoop.

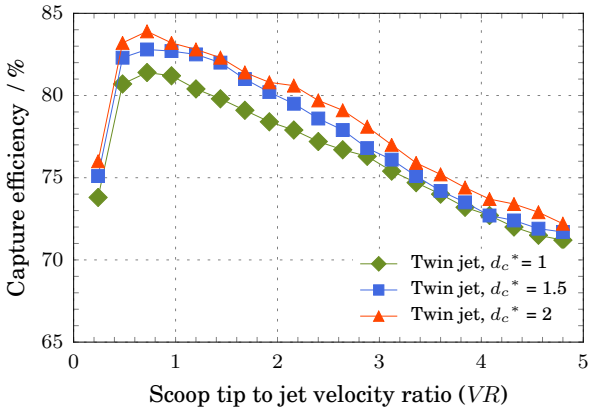

Fig. 17: Effect of constriction on capture efficiency for fixed jet velocity and varying shaft speed.

5.3 Jet velocity varying with shaft speed

In these tests the velocity ratio ($VR = \frac{R_{tip}\omega}{V_j}$) had values between 4.4 and 4.8 as shown in Fig. 18. Over a significant portion of the shaft speed range the velocity ratio was constant at around 4.4. The measured capture efficiency over the range of shaft speeds increases with shaft speed and is slightly higher when the scoop constrictions ratio d_c^* is 2 compared to 1 or 0.5 (73% at ω/ω_{max}=1 compared to 71% for the smaller constrictions). Capture efficiency values are around 60% to 70%, slightly lower than the values obtained for the same velocity ratio (but a higher jet velocity) as shown in Fig. 17 where a velocity ratio of 4.4 corresponds to a capture efficiency of around 72% in the case of constriction ratio of 1. Fig. 18 provides confirmation that constriction does not make a lot of difference to capture efficiency. The fact that the larger constriction ratio of 2 has slightly better capture efficiency than the smaller values 1 or 0.5 would suggest that there is an element of the constriction preventing oil moving past the constriction as fast as it would like to but that this is a minor effect.

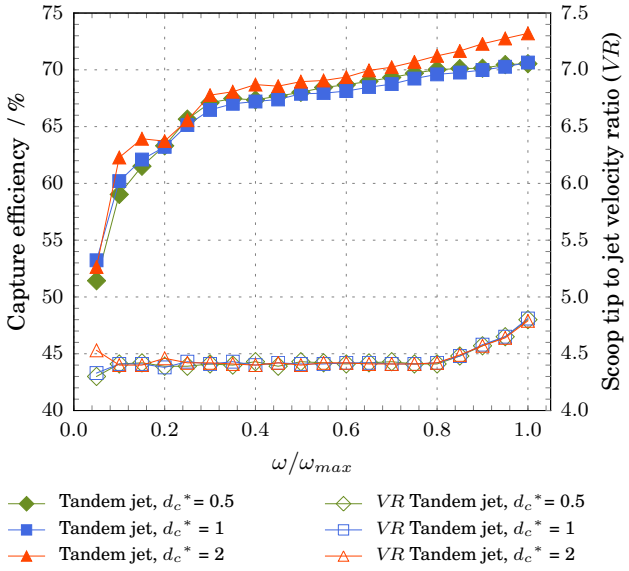

Fig. 18: Graph showing how capture efficiency varies with shaft speed for three constriction values. Velocity ratios as plotted on the chart.

A second set of tests was done with a somewhat higher velocity ratio at higher shaft speeds and the data is shown on Fig. 19. As can be seen, with the higher velocity ratios the capture efficiency falls a little. This is indicative that for the same shaft speed, slightly less oil is retained by the scoops when the jet velocity is lower. This is consistent with the findings of Prasad et al [10] and with the identified importance of jet momentum in opposing centrifugal force.

All three jet configurations are compared in the data shown in Fig. 20, for a constriction ratio of 1 and velocity ratios as shown on the chart. Here it is clear that the twin and tandem jets behave in a very similar fashion but lower capture efficiencies are obtained for the single jet. As shown in Fig. 15 the front part of the jet deflects after hitting the scoop and is then flattened by the aerodynamic forces creating a low pressure region in the vicinity of the scoop tip. With the tandem jet the second jet does not see the same pressure field as the front jet and the deflection a) happens earlier and b) much of the deflected oil meets the front jet and is still captured. To some extent this can be seen in Fig. 21, which shows images for all three jets at a shaft speed ratio of 1. With the twin jet, although behaviour is less clear, it seems that the deflection of the two jets is reduced because of their proximity. At higher speed the still images are less clear as can be seen in Fig. 22 where the shaft speed ratio is 0.8, but it can be seen that the single jet case shows a more sheet-like deflection of the jet compared to the twin jet. It is suggested that the interaction of the jets creates a flow less susceptible to deflection.

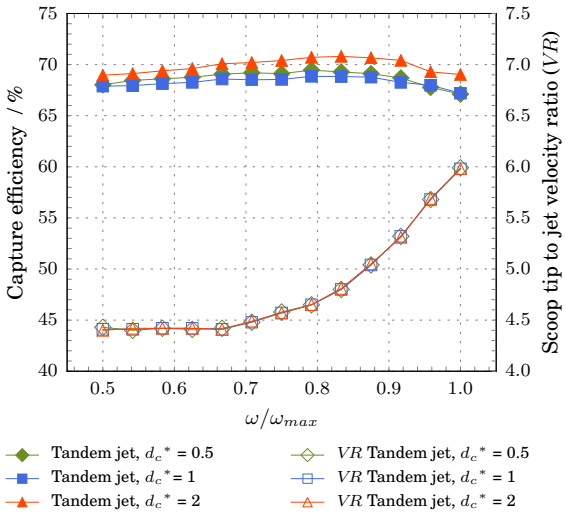

Fig. 19: Capture efficiency as a function of shaft speed for three constrictions values and velocity ratios as indicated on the chart.

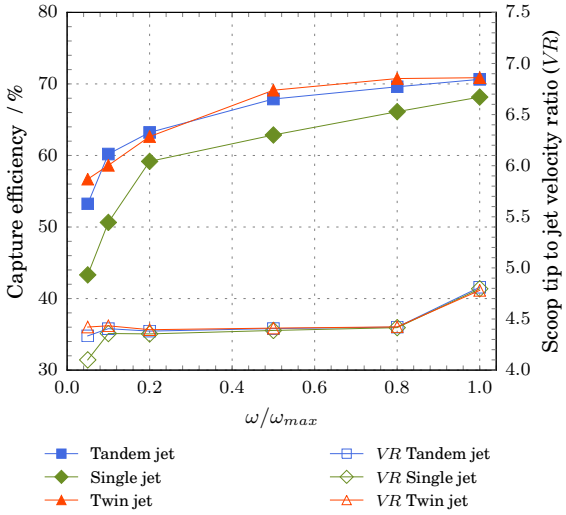

Fig. 20: Graph showing the effect of jet configuration for a case with 2mm constriction and velocity ratios as shown in Fig. 18.

5.4 Effect of jet angle

The effect of jet angle was evaluated for the baseline jet orientation, θ_{ref}, and the angles $\theta_{ref}-5^\circ$ and $\theta_{ref}-10^\circ$. Three scoop constrictions were assessed over shaft speeds ratios from 0.5 to 1, at the same velocity ratios as indicated in Fig. 19. The capture efficiency characteristics are shown in Fig. 23. It can be seen that decreasing the jet angle from baseline increases the capture efficiency with maximum values around 79% being obtained at $\theta_{ref}-10^\circ$ and 76% at $\theta_{ref}-5^\circ$ compared to the maximum around 69% for baseline θ_{ref}. These three values are valid for the constriction ratio of 1.

The increase of the capture efficiency with decreasing jet angle, may be attributed to changes of a) the momentum

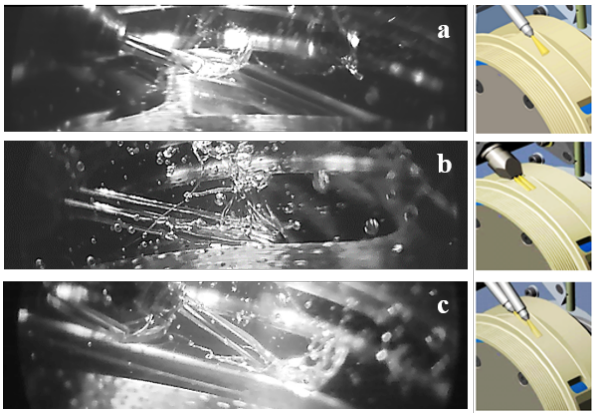

Fig. 21: Visualization of the jet flow behaviour at the shaft speed ratio of 0.1 for three different jet configurations: a) single jet, b) twin jet and c) tandem jet.

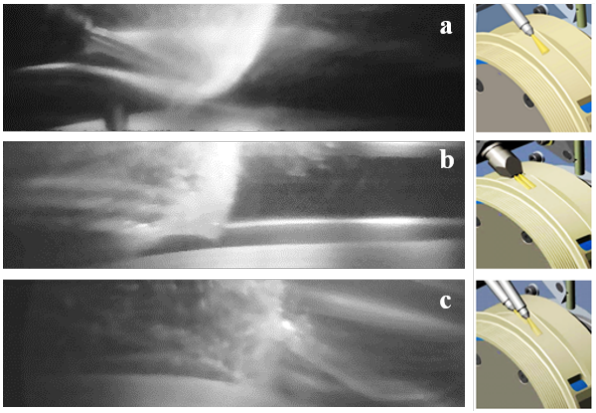

Fig. 22: Visualization of the jet flow behaviour at the shaft speed ratio of 0.8 for three different jet configurations: a) single jet, b) twin jet and c) tandem jet.

and b) the deflection of the oil jet.

With regard to momentum, the simplified diagrammatic representation of Fig. 24 shows how the location where the oil jet impacts on the scoop changes with the jet angle. Reducing the jet angle from the baseline, the oil jet strikes more inboard from the scoop tip and closer to the constriction as is illustrated in Fig. 24a. In that case the flow path of the oil film spread against the scoop is shorter, before it reaches the constriction. It may therefore be expected that the oil film loses less momentum and is therefore less likely to be ung back off the scoop. Thus the amount of lost oil is reduced, which could partially account for the increase in the capture efficiency.

With regard to oil jet deflection it is found that after slicing the jet is less deected at lower jet angles, as is shown by the images of Fig. 25. Fig. 25a (i) shows the jet when it is about to hit the edge of the scoop. It is notable that in the region radially outside the scoop that is approaching the jet, there is a cloud of ligaments and drops of oil (highlighted in a circle) and these are the oil coming from the plume created during the previous scoop-jet interaction. This is oil which

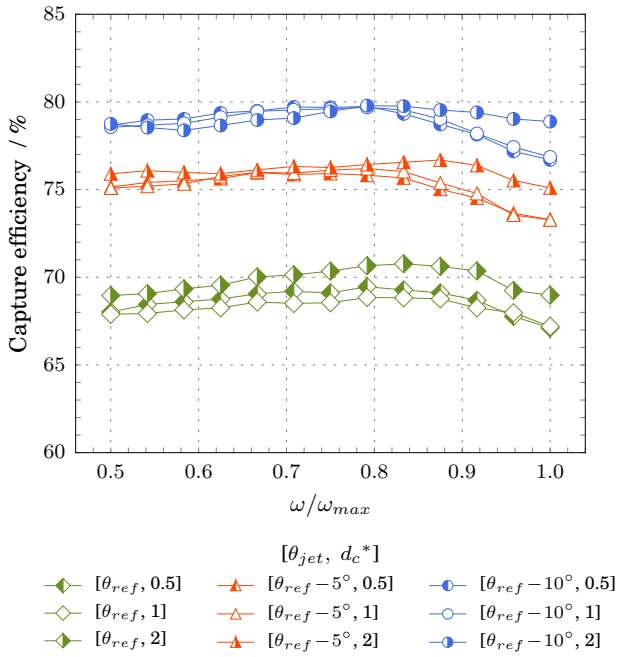

Fig. 23: Effect of jet angle on capture efficiency for three scoop constrictions for the tandem jet configuration.

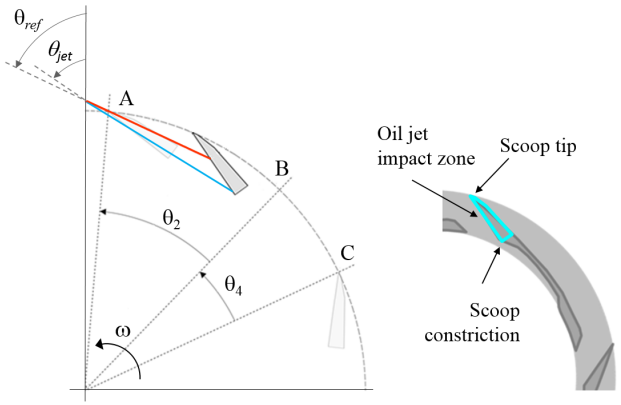

Fig. 24: Position where oil jet impacts on the scoop at different angles. Scoop operating with $VR \geq VR_{thr}$ (a) at the baseline jet angle θ_{ref} (red line) and at a jet angle lower than the baseline, $\theta_{jet} < \theta_{ref}$ (blue line). (b) Key zones of the simplified scoop geometry.

has not been captured by the scoop and is now mixing with the expelled oil. Fig. 25a (iii) shows how the jet after hitting the scoop evolves into a big plume with a jet deflection angle α of approximately 135 ° from the baseline jet angle. This plume expands outwards with formation of ligaments that will not be captured by the next scoop. When the baseline jet angle is reduced by 5° as shown in Fig. 25b(i) there is no trace of oil escaping as a consequence of plume formation, and there is only expelled oil visible. After hitting the scoop edge (Fig. 25b(iii)), the jet deflection angle is about zero and therefore the plume is much less deflected and so travels along with the jet. The same holds for the ligaments which move parallel to the jet and are therefore captured by the next scoop.

The capture efficiency was also measured for a shaft speed ratio of 0.05, VR of 4.3 and constriction ratio of 1 yielding 51% and 59% for the baseline jet angle and for θ_{ref} $-5°$ respectively.

From visualization at high speed it was also observed that for the baseline jet angle the flow was deflected more severely than for lower jet angles. At the higher speeds the flow visualization was hindered by splashing which affects the quality of the still images which are therefore not shown in the paper but considerable insight was obtained through viewing the movies.

It is also interesting to note that whereas at baseline jet angle θ_{ref} there is roughly a 2% advantage of the constriction ratio of 2 over 1, this is not seen for $\theta_{ref}-10°$ except at the highest shaft speeds where the velocity ratios were highest.

Fig. 25: Comparison of oil deflected after hitting the edge of the scoops for the tandem jet configuration and two jet angles: (a) Baseline jet angle θ_{ref} and (b) θ_{ref} $-5°$ jet angle. The evolution of the jet flow is shown 1×10^{-3}s before the jet hits the edge of the scoop, during the slicing action at t_i and 3×10^{-3}s after hitting the edge of the scoop. Images arfe for shaft speed ratio 0.05, VR 4.3 and constriction ratio 1. The blue arrow points to the leading edge of the scoop.

5.5 Further considerations and future work

For the experiments conducted in this study air conditions were ambient and oil supply temperature was lower than would be found in an aeroengine bearing chamber. This facilitated the high quality visualisation central to the experimental work conducted. However, it is necessary to evaluate how the flow behavior might be different at more engine representative conditions. Taking generic representative bearing chamber conditions of pressure 2.6 bar, air temperature

280° and oil temperature 160° we obtain a test rig oil Weber number around 16% lower than in an engine and an air Weber number around 50% lower. The oil Reynolds number is around 90% of the engine value. These differences primarily arise due to reduced oil viscosity at higher temperatures. The biggest influence of these differences will be in the number and size of droplets produced by jet-scoop impact. Primary oil jet capture by the scoop is not dominated by droplet splashing and so there is no reason to doubt the applicability of the main findings presented here.

One of the important benefits of this experimental work comes from data made available for numerical model validation and indeed G2TRC have conducted both CFD and SPH modelling on scoops. Consequently, building on the work of [11] a CFD model with modified oil and air properties could relatively easily be created. Future experimental work could be conducted at higher temperature and pressure but a new test module (likely with significantly reduced visual access) would be required and so future CFD investigation is recommended prior to future experiments. It is also worth noting that a numerical investigation using smooth particle hydrodynamics has investigated the effect of oil viscosity and shown it to have a negligible effect on predicted capture efficiency [12].

The work presented here shows that a scoop system of this type is capable of capturing the majority of the oil delivered by the jet over a range of representative shaft speeds and oil flowrates. It can be argued that 100% capture is not desirable in any case as some oil may be required for wetting the walls of the chamber where the oil is delivered. The size of the constriction has been shown to be important but results are not so sensitive that differential thermal expansion will prevent adequate oil delivery over an engine operation envelope. It seems therefore that the proposed system has considerable promise for future engine applications and future work may involve testing on an engine or a more engine representative test rig.

6 Conclusions

An experimental investigation into a scoop geometry has been conducted to measure the capture efficiency of a system with the potential for delivering oil to transmissions components in a gas turbine engine at a different axial location to the feed jet. Geometric variations of the oil jet injector and the scoop over a range of operating conditions have been examined.

A simplified geometrical model is presented that introduces the capture criterion and provides valuable insight into how geometric and operational parameters affect the system's behaviour. This model shows that for any scoop operating at a velocity ratio above the total capture threshold $VR \geq VR_{thr}$, the oil jet is theoretically entirely captured and thus the theoretical capture efficiency is 100%. In practice total capture is not achieved, with the highest observed value being 81% occurring at a velocity ratio between 0.8 and 1. This was measured at high jet velocity with the twin jet configuration and baseline jet angle and constriction. At higher velocity ratios (further increase of shaft speed) there is reduced capture efficiency. The cause of reduction from the theoretical efficiency is that in this latter case, the motion of the fluid is described without consideration of effects such as oil deflection, plume formation, oil shedding as ligaments and drops nor oil ejected outwards from the scoop as a consequence of centrifugal forces all of which represent oil lost to the system.

Effect of scoop constriction, fixed jet velocity. Increasing the constriction from the baseline case to constriction ratios of 1.5 and 2, for fixed high jet velocity was investigated using the twin jet configuration. Capture efficiencies show similar behaviour presenting the maximum efficiency at similar velocity ratios between 0.8 and 1. The effect of increasing the constriction has a very small impact on the maximum capture efficiency particularly in going from 1.5 to 2, where the difference falls within experimental uncertainty. There is an improvement of 2.5% from baseline case to constriction ratio of 2.

Jet velocity varying with shaft speed. With an almost constant velocity ratio of around 4.4 the capture efficiency increases with increasing shaft speed attaining values around 60% to 70%. These values are slightly lower than those obtained for the same velocity ratio but a higher jet velocity (for example 72% when constriction ratio was 1). When the velocity ratio was increased by reducing the jet velocity for the same shaft speed, the capture efficiency reached its maximum value at a velocity ratio of around 4.8 and then fell for higher shaft speeds. Less oil is retained when the jet velocity is lower. A tentative conclusion from these results is that if a smaller nozzle diameter can be tolerated (maintaining flowrate and thus increasing velocity) then higher capture efficiencies will be achieved. Reducing the constriction ratio from 1 to 0.5 did not have any significant effect on the measured capture efficiency. Slightly higher values were obtained when the constriction ratio was increased to 2.

Comparison of jet configurations. For the three jet configurations investigated the two-jet configurations (tandem and twin jets) presented similar capture efficiency while for the single jet configuration the efficiency was lower by around 10% at low shaft speeds and 3% at high shaft speeds. Therefore jet configurations involving two jets are recommended for a higher capture efficiency.

Effect of jet angle. The angle of the oil jet is identifed as a key parameter to consider when designing a scoop feed system. The capture efficiency increased by around 11% when the jet baseline angle was reduced by 10°. Funding in this project did not permit exploration of other jet angles so further work is recommended to identify the optimum jet angle for the scoop system.

Overall this study establishes the capability of a scoop system of this kind to capture and retain oil delivered via a feed jet. The work shows that it is not viable to capture all the jet oil because of jet pluming and splashing but careful choice of geometric and operational parameters can yield signficant improvement. In particular lower velocity ratio (higher jet velocity) is shown to be advantageous and choice of jet angle is a key design parameter. Further investigation

starting with numerical modelling is recommended but the authors see no reason why such a system should not be trialled at engine-representative conditions.

Acknowledgements

The authors would like to thank Rolls-Royce plc for its financial and technical support and the UK Technology Strategy Board for its financial support of the SILOET 2 Program.

References

[1] Zaretsky, E. V., 1997. "Rolling Bearing and Gear Lubrication". *Tribology for Aerospace Applications*. Society of Tribologists and Lubrication Engineers, Park Ridge, Ill., US, pp. 207-323.

[2] Brown, P. F., 1970. "Bearings and Dampers for Advanced Jet Engines". SAE Technical Paper No. 700318, Warrendale, Pennsylvania, US.

[3] Lee, C. W., Johnson, G. R., Palma, P. C., Simmons, K., and Pickering, S. J., 2004. "Factors Affecting the Behaviour and Efficiency of a Targeted Jet Delivering Oil to a Bearing Lubrication System". Proceedings of ASME Turbo Expo 2004, Vienna, Austria, ASME Paper No. GT2004-53606, Vol. **2**, pp.191–199.

[4] Kovaleski, S., 1987. "Radial Scoop Construction". US Patent 4,648,485.

[5] Fisher, K., Demel, H., and Hazeley, R., 2002. "Methods and Apparatus for Supplying Oil to Bearing Assemblies". US Patent 6,409,464.

[6] Fisher, K., 2004. "Bi-Directional Oil Scoop for Bearing Lubrication". US Patent 6,682,222.

[7] Dins, J., Hogan, J., and Kumar, A., 2007. "Curved Blade Oil Scoop". US Patent 7,244,096.

[8] Mcdonagh, S., 2016. "A Liquid-Capturing Shaft". US Patent 2016/0069186 A1.

[9] RAEng, 2014. "Innovation in Aerospace". Royal Academy of Engineering in association with the Royal Aeronautical Society, London, UK, http://www.raeng.org.uk.

[10] Prasad, S. K., Sangli, P., Buyukisik, O., and Pugh, D., 2014. "Prediction of Gas Turbine Oil Scoop Capture Efficiency". Proceeding of ASME 2014 Gas Turbine: Power for Land, Sea and Air, New Delhi, India, ASME Paper No. GTINDIA2014-8329, pp. V001T05A004 1-8.

[11] Korsukova, E., Kruisbrink, A., Morvan, H., Cageao, P. P., and Simmons, K., 2016. "Oil Scoop Simulation and Analysis using CFD and SPH". Proceding of ASME Turbo Expo 2016: Turbine Technical Converence and Exposition, Seoul, South Korea, ASME Paper No. GT2016-57554, Vol. **7B**, pp. V07BT31A027 1-8.

[12] Kruisbrink, A., Korsukova, E., Evans, K., and Morvan, H. P., 2017. "SILOET 2 Project 18.4: CFD and SPH Work on the Compound Scoop". Gas Turbine and Transmissions research centre, University of Nottingham.